Applied Physics Letters

RESEARCH ARTICLE | JUNE 03 2024

Switching of major nonradiative recombination centers (NRCs) from carbon impurities to intrinsic NRCs in GaN crystals

K. Sano ; H. Fujikura ; T. Konno ; S. Kaneki ; S. Ichikawa ; K. Kojima

Appl. Phys. Lett. 124, 231101 (2024)
https://doi.org/10.1063/5.0207339

AIP Publishing

Applied Physics Letters ARTICLE pubs.aip.org/aip/apl

Switching of major nonradiative recombination centers (NRCs) from carbon impurities to intrinsic NRCs in GaN crystals

Cite as: Appl. Phys. Lett. **124**, 231101 (2024); doi: 10.1063/5.0207339
Submitted: 7 March 2024 · Accepted: 6 May 2024 ·
Published Online: 3 June 2024

View Online Export Citation CrossMark

K. Sano,[1,a)] H. Fujikura,[2] T. Konno,[2] S. Kaneki,[2] S. Ichikawa,[1] and K. Kojima[1]

AFFILIATIONS

[1]Graduate School of Engineering, Osaka University, Suita, Osaka 565-0871, Japan
[2]Sumitomo Chemical Co. Ltd., Hitachi, Ibaraki 319-1418, Japan

[a)]Author to whom correspondence should be addressed: koshi.sano@sfm.eei.eng.osaka-u.ac.jp

ABSTRACT

The external quantum efficiency (EQE) and internal quantum efficiency (IQE) of radiation are quantified by omnidirectional photoluminescence measurements using an integrating sphere for two types of GaN crystals with different carbon concentrations ([C] = 1×10^{14} cm^{-3}, 2×10^{15} cm^{-3}). In the sample with lower [C], when the excitation density is 140 W cm^{-2}, the EQE and IQE for near-band-edge (NBE) emission are 0.787% and 21.7%, respectively. The relationship between [C] and the IQE for NBE emission indicates that carbon impurities work as effective nonradiative recombination centers (NRCs) in n-type GaN, and major NRCs switch from carbon impurities to intrinsic NRCs, such as vacancies, when [C] falls below 3.5×10^{14} cm^{-3}.

Developing highly efficient optical and electronic devices that reduce total energy consumption is essential for a sustainable society. After the wide spread of indium gallium nitride (InGaN)-based blue and white light-emitting diodes with the external quantum efficiency (EQE) exceeding 80%,[1] gallium nitride (GaN)-based power devices have now attracted significant attention. GaN is a suitable material for power devices due to its excellent physical properties such as large bandgap energy (3.4 eV), high breakdown field (3.3 MV/cm),[2] and high saturation electron velocity (2.5×10^7 cm/s).[3] At high threading dislocation (TD) density from 10^8 to 10^{10} cm^{-2}, TDs work as major nonradiative recombination centers (NRCs), which reduce the efficiency of near-band-edge (NBE) emission. Hence, TDs are a factor in device performance degradation.[4] In recent years, GaN crystals with TD density less than 10^6 cm^{-2} have been commercially available due to remarkable improvements in GaN crystal growth technology.[5–16] In such crystals, the average distance between TDs is more than 10 μm, while the minority carrier diffusion length is the order of 1 μm.[17–19] This means that the major NRCs attributed to point defects, such as vacancies or impurities, rather than TDs.

Carbon impurities, a sort of extrinsic point defects in GaN, are well-known to degrade the performance of GaN-based devices by forming deep levels (DLs) in the bandgap. For example, carbon impurities in the n-type GaN work as Shockley–Read–Hall (SRH) type NRCs, which reduce the efficiency of NBE emission. In addition, variations in the in-plane resistivity of n-type[20] and p-type[21] *c*-plane GaN have been reported. Such an inhomogeneity in resistivity is attributed to variations in the in-plane carbon concentration ([C]). Therefore, understanding carbon-related DLs is critical to improve the reliability of GaN-based devices. Carbon impurities in GaN are expected to preferentially occupy N-lattice sites because the formation energy of C substituting on the N site (C_N) is about 2.0 eV, whereas those of C substituting on the Ga site (C_{Ga}) and a single interstitial impurity (C_i) are more than 5.0 eV.[22,23] Several reports have comprehensively investigated the formation energies of complexes as well as single carbon impurities in GaN using first-principles calculations that employed a hybrid density functional theory.[23,24] It has been reported that under thermal equilibrium at typical growth temperatures, the concentration of C_N is an order of magnitude higher than that of defect complexes due to the lower binding energy of the complex compared to isolated C_N.[24] Therefore, in this study, we focus on a single C_N. The recent hybrid density functional theory indicates that C_N is not a shallow acceptor but a deep acceptor with the 0/− transition level at $E_v + 0.90$ eV.[22,25]

From an experimental perspective, photoluminescence (PL) spectroscopy has been widely used to study the effect of carbon impurities on the optical properties of GaN.[26–35] The yellow

luminescence (YL) band peaking at about 2.2 eV is known as the defect-related PL band in undoped and C-doped n-type GaN.[26,27,29,31] Furthermore, electrical properties have been investigated mainly using deep level transient spectroscopy (DLTS).[36–45] The characteristics of the H1 hole trap commonly observed at 0.85–0.90 eV above E_v by DLTS are in good agreement with the acceptor level of C_N.[38,39,41–43]

The metalorganic vapor phase epitaxy (MOVPE) and halide vapor phase epitaxy (HVPE) methods are widely used for GaN growth technology. In the MOVPE method, carbon contamination is inevitable due to the use of organometallics as precursors, and even with manipulation of growth parameters, [C] is approximately $2-4\times10^{15}\,\mathrm{cm^{-3}}$.[16,46] Also, in MOVPE GaN, there is a trade-off between the electron trap E3 ($E_v+0.60$ eV) and carbon, and their simultaneous reduction is difficult.[39,40] Recent detailed studies have revealed that the origin of the E3 trap is the 0/– state of Fe occupying the Ga sites.[44,45] Therefore, the trade-off between [E3] and [C] in MOVPE GaN can be explained in terms of the inverse dependence of C and Fe uptake efficiency on MOVPE growth parameters. The HVPE method is one of the most effective methods for preventing carbon contamination.[10] Recently, GaN crystals with extremely low carbon concentrations ($[C]=1\times10^{14}\,\mathrm{cm^{-3}}$) have been achieved by the quartz-free HVPE (QF-HVPE) method, which removes the quartz parts from the high-temperature region of the reactor.[47] The QF-HVPE method overcomes the trade-off between [E3] and [C] by controlling the etching of the stainless steel flange. Although high donor concentration due to silicon and oxygen contamination is known in HVPE GaN,[8] the QF-HVPE method overcomes this problem ([Si], $[O]<5\times10^{14}\,\mathrm{cm^{-3}}$). For QF-HVPE GaN, the agreement between [H1] and [C], and the N_d-N_a values evaluated from capacitance–voltage (C–V) measurements (N_d and N_a are donor and acceptor concentrations, respectively) and [Si]–[C], has been reported.[42,47]

In general, secondary ion mass spectrometry (SIMS) is used to quantify [C].[48–50] However, its detection limit is $1\times10^{14}\,\mathrm{cm^{-3}}$ even with the highly sensitive raster changing method.[48] Compared to SIMS measurements, PL spectroscopy is attractive to determine [C] because it is nondestructive, non-contact, and does not require electrodes for measurements. However, general PL measurements do not allow the absolute quantification of the two types of quantum efficiency (QE), i.e., EQE and internal QE (IQE) for the NBE emission. This is because general PL measurements do not detect all PL photons, but only detect those coupled to the collecting lens. The IQE is given by $\tau_R^{-1}/(\tau_R^{-1}+\tau_{NR}^{-1})$, where τ_R and τ_{NR} are the radiative and nonradiative recombination lifetimes, respectively. In this study, nonradiative recombination is defined as recombination that does not contribute to the NBE emission. Therefore, defect-induced transitions, such as YL, are also considered as nonradiative recombination. Using the capture cross-section for minority carrier (σ), the thermal velocity of minority carrier (v_{th}), and the concentration of nonradiative recombination center (N_{NRC}), τ_{NR}^{-1} is expressed by $\sum\sigma\cdot v_{th}\cdot N_{NRC}$. As described above, the IQE for NBE emission is limited by the τ_{NR}, and the τ_{NR} is directly related to N_{NRC}. Therefore, the IQE for NBE emission is a good indicator to evaluate crystal quality. We have developed omnidirectional photoluminescence (ODPL) spectroscopy using an integrating sphere to quantify EQE and IQE values absolutely. It has been shown that [C] and the QE for NBE emission are strongly correlated based on ODPL measurements.[35]

In this Letter, ODPL measurements are performed at room temperature for two samples with different [C] ($1\times10^{14}\,\mathrm{cm^{-3}}$ and $2\times10^{15}\,\mathrm{cm^{-3}}$). The relationship between [C] and QE are quantitatively shown together with the results of previous measurements. These results indicate that carbon works as the major NRCs in most ranges of [C] from 1×10^{14} to $2\times10^{16}\,\mathrm{cm^{-3}}$, and when [C] falls below $3.5\times10^{14}\,\mathrm{cm^{-3}}$, complex vacancies work as the major NRCs rather than carbon.

A schematic of the ODPL measurement is shown in Fig. 1. The ODPL spectroscopy measures light emitted from all directions using an integrating sphere.[51] Details of the two samples measured in this study are shown in Table I. The GaN crystals are approximately 450 μm thick, grown by the QF-HVPE method on Si-doped c-plane GaN substrates with an off-angle of 0.3 degrees. GaN substrates have an uniform TD density from 1×10^6 to $3\times10^6\,\mathrm{cm^{-2}}$. The concentrations of transition metal impurities, such as Fe, Mn, and Cr, which are known to work as effective SRH-type NRCs,[52] were below the detection limit of SIMS analysis ([Fe], [Mn] $<5\times10^{14}\,\mathrm{cm^{-3}}$, [Cr] $<1\times10^{14}\,\mathrm{cm^{-3}}$). The ODPL measurements were performed for HV1 with [C] of $2\times10^{15}\,\mathrm{cm^{-3}}$ and HV2 with [C] of $1\times10^{14}\,\mathrm{cm^{-3}}$. Here, the impurity concentrations and N_d-N_a values for two samples were quantified by the SIMS raster changing method and C–V measurements, respectively. As described above, we consider that N_d is derived from silicon because [Si]–[C] and N_d-N_a are in good agreement for QF-HVPE GaN. For the excitation of PL, a continuous wave (CW) laser was used with the photon energy (E) of 3.87 eV. All measurements were performed at room temperature and with the integrating sphere in ambient nitrogen to prevent PL intensity attenuation.[53]

Typical ODPL spectra of HV1 and HV2 are shown in Fig. 2, where the spectra consist of at least three bands. Band A with 1.38 eV $<E<$ 2.52 eV consists mainly of green luminescence (GL), YL, and red luminescence (RL) bands. Band B with 2.52 eV $\le E\le$ 3.04 eV consists mainly of a blue luminescence (BL) band. The NBE emission is 3.04 eV $<E<$ 3.54 eV. For the RL band around 1.8 eV, the origin is not clear, while there are reports that it has been observed in HVPE-grown GaN with [C] down to $1\times10^{15}\,\mathrm{cm^{-3}}$.[34,54] Note that the higher intensity in HV2 than in HV1 is not only simply due to more RL-related DLs but also due to re-excitation to such levels by the photon recycling (PR) effects, in which photons generated by radiative recombination are self-absorbed and experience reincarnation as photons.[55,56] This re-excitation of DLs due to the PR effect is also true

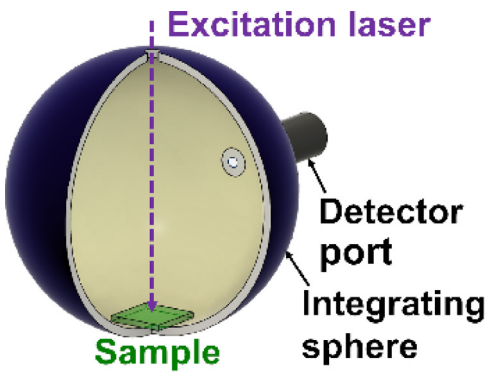

FIG. 1. Schematic of the ODPL measurement (2π configuration).

TABLE I. Carbon and net donor concentrations.

Sample ID	[C] ($\times 10^{15}$ cm^{-3})	$N_d - N_a$ ($\times 10^{15}$ cm^{-3})
HV1	2.0	2.0
HV2	0.1	4.0

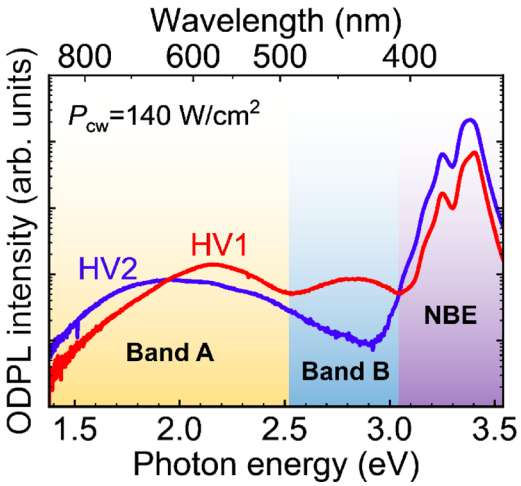

FIG. 2. Typical ODPL spectra of HV1 and HV2 under the cw excitation at room temperature. The spectra consist of band A with 1.38 eV $< E <$ 2.52 eV, band B with 2.52 eV $\leq E \leq$ 3.04 eV, and NBE emission with 3.04 eV $< E <$ 3.54 eV.

for YL-, GL-, and BL-related DLs. For the YL band around 2.2 eV, which is commonly observed in n-type GaN crystals, although early first-principles calculations strongly supported V_{Ga} defects or $V_{Ga}O_N$ complexes as the cause of the YL band,[57,58] recent calculations predict that the YL band is rather due to C_N.[22,25] Since HV1 and HV2 are grown by the QF-HVPE method and the oxygen concentration is below the detection limit of SIMS analysis ([O] $< 5 \times 10^{14}$ cm^{-3}), the origin of the YL bands in HV1 and HV2 is probably carbon. For the GL band around 2.4 eV, a nitrogen vacancy (V_N) has been pointed out as the origin by using the first-principles calculations.[32] For the BL band around 2.9 eV, several researchers have reported that the BL band is observed in high carbon-doped GaN crystals.[28,30,33] As for the origin of the BL band, the +/0 transition level of C_N ($E_v + 0.35$ eV) has been pointed out using first-principles calculations.[22] The ODPL spectra for the NBE emission have a double-peak structure with a trough at the fundamental absorption edge ($E_{abs} = 3.31$ eV). This is because the light extraction efficiency (LEE, η^L) for $E < E_{abs}$ is significantly higher than that for $E > E_{abs}$ due to the existence of the Urbach tail.[59] In the ODPL measurements, such double-peaked structures are commonly observed in direct bandgap semiconductors such as $CH_3NH_3PbBr_3$[60] and ZnO bulk crystals.[61] The ratio of the low-energy side of the double peak is larger in HV2 because the PR effect increases the light outcoupling on the low-energy side.

The EQE values of both samples are shown as a function of excitation density (P_{cw}) in Fig. 3 for (a) band A, (b) band B, and (c) NBE emission. The EQE values for bands A and B are independent of P_{cw}, while the EQE values for NBE emission monotonically increase with the increment of P_{cw}. In HV1, the EQE values for NBE emission increase from 0.022% to 0.250% when P_{cw} increases from 2.8 to 140 W cm^{-2}. In HV2, the EQE values for NBE emission increase from 0.017% to 0.787% when P_{cw} increases from 0.9 to 140 W cm^{-2}. At all excitation densities, there is a clear difference in the EQE values for NBE emission between HV1 and HV2, even when an experimental error was taken into account. Meanwhile, the EQE values for bands A and B show little difference between HV1 and HV2.

Figure 4 shows the relationship between [C] and the EQE values for NBE emission when P_{cw} is 140 W cm^{-2}. The other data of the EQE values are the previous results.[35] Since the EQE values for NBE emission increase monotonically with decreasing [C] with the EQE = 0.02% (0.787%) at [C] = 2×10^{16} cm^{-3} (1×10^{14} cm^{-3}), carbon impurities work as effective NRCs and reduce the EQE value for NBE emission. Here, the experimental errors are small enough for the figure plots when P_{cw} is 140 W cm^{-2} [same for Fig. 5(a)].

The IQE values for NBE emission at P_{cw} of 140 W cm^{-2} are shown in Fig. 5(a) as a function of [C]. In ODPL measurements, the EQE value for NBE emission can be converted to IQE by introducing a direct external quantum efficiency (η') where the escape channel is limited by the upper-half escaping cone.[51] The IQE value (η) for NBE emission considering the PR effect can be expressed as $\eta = \eta'/[\eta' + (1 - \eta')\eta^L]$ using LEE (η^L) and η'. In GaN, the LEE value was estimated to be 2.55%, taking into account the refractive index difference between GaN and air.[51] As described above, the IQE can be expressed as

$$\eta = \frac{\tau_R^{-1}}{\tau_R^{-1} + \sum \sigma \cdot v_{th} \cdot N_{NRC}}. \quad (1)$$

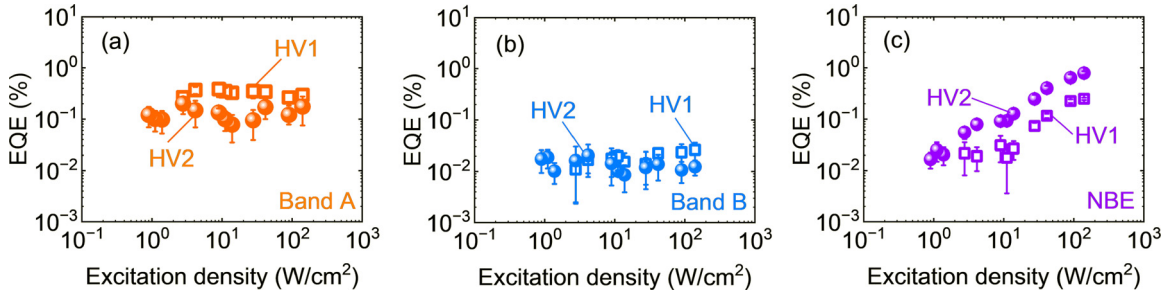

FIG. 3. The EQE values of both samples as a function of P_{cw} for (a) band A, (b) band B, and (c) NBE emission.

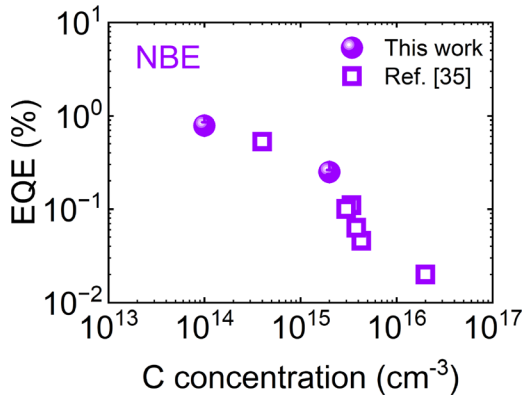

FIG. 4. Relationship between [C] and the EQE values for NBE emission when P_{cw} is 140 W cm^{-2}. Results of this work are shown in circles and previous results[35] are shown in squares. Reproduced with permission from Kojima *et al.*, Appl. Phys. Express **13**, 012004 (2019). Copyright 2019 Applied Physics Express.

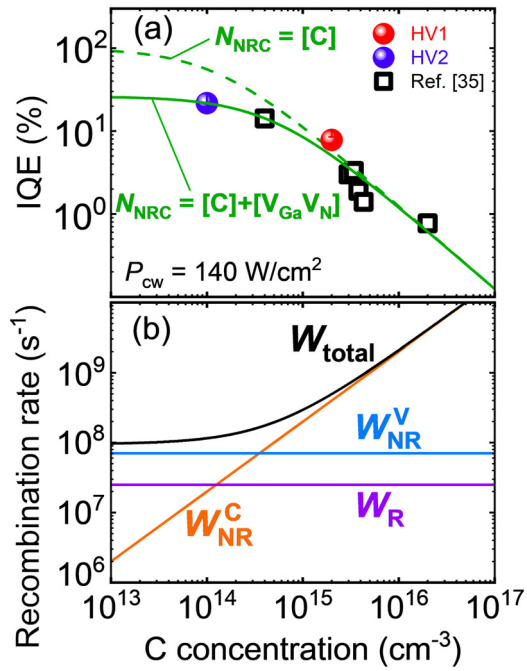

FIG. 5. (a) The IQE values for NBE emission at P_{cw} of 140 W cm^{-2} as a function of [C]. Results of this work are shown in circles and previous results[35] are shown in squares. Reproduced with permission from Kojima *et al.*, Appl. Phys. Express **13**, 012004 (2019). Copyright 2019 Applied Physics Express. (b) Relationship between [C] and recombination rate assuming common $\sigma_V \cdot \nu_{th} = 6.4 \times 10^{-7}$ cm^3/s (Ref. 62) and [$V_{Ga}V_N$] = 1.1×10^{14} cm^{-3}.

The dashed curve in Fig. 5(a) is the result of using $\sigma_C \cdot \nu_{th} = 2.0 \times 10^{-7}$ cm^3/s,[35] $\tau_R = 40$ ns,[63,64] and N_{NRC} = [C] in Eq. (1). The IQE values increase monotonically with decreasing [C] as well as the EQE values for NBE emission. In most ranges of [C] from 1×10^{14} to 2×10^{16} cm^{-3}, the results of ODPL measurements and analytical solutions are good agreements. This result indicates that carbon impurities can work as effective NRCs in n-type GaN crystals. The EQE and IQE values for NBE emission are extremely sensitive to [C], so those values can be used for the calibration of [C] in this range. The IQE value for HV2 is 21.7%, breaking the previous value of 14.2%.[35] However, the result is below the fitted curve. This disagreement suggests that the presence of major NRCs other than carbon in HV2. One possibility is intrinsic NRCs formed by $V_{Ga}V_N$. This divacancy is observed in n-type GaN crystals and works as an SRH type NRCs.[62] Surface recombination is another possibility. Although the material is different, there is a report that InGaN has an extremely long surface recombination lifetime (3.8 ns) due to surface band-bending.[65] We believe that such surface band-bending also exists in GaN and consider only $V_{Ga}V_N$ in this study. In HV2, [$V_{Ga}V_N$] can be estimated to be 1.1×10^{14} cm^{-3}, using $\sigma_V \cdot \nu_{th} = 6.4 \times 10^{-7}$ cm^3/s.[62] The relationship between [C] and [$V_{Ga}V_N$] is unclear and should be discussed in detail in the future. The solid curve in Fig. 5(a) is the result of using $\sigma_V \cdot \nu_{th} = 6.4 \times 10^{-7}$ cm^3/s, [$V_{Ga}V_N$] = 1.1×10^{14} cm^{-3}, and N_{NRC} = [C] + [$V_{Ga}V_N$] in Eq. (1), respectively. The relationship between [C] and each recombination rates are shown in Fig. 5(b). Here, the radiative recombination rate (W_R), the nonradiative recombination rate by carbon (W^C_{NR}), and the nonradiative recombination rate by $V_{Ga}V_N$ (W^V_{NR}) are τ_R^{-1}, $\sigma_C \cdot \nu_{th} \cdot$ [C], and $\sigma_V \cdot \nu_{th} \cdot$ [$V_{Ga}V_N$], respectively. In all [C] ranges, the radiative recombination rate is never dominant. In the high [C] range, the nonradiative rate by carbon converges asymptotically to the total recombination rate. However, below [C] = 3.5×10^{14} cm^{-3}, the nonradiative recombination rate by $V_{Ga}V_N$ becomes dominant. Thus, major NRCs switch from carbon to intrinsic NRCs, such as divacancy, when [C] falls below 3.5×10^{14} cm^{-3}.

In conclusion, the relationship between [C] and the QE for NBE emission is quantitatively shown based on ODPL measurements. In HV2, the EQE and IQE values for NBE emission is 0.787% and 21.7%, breaking the previous value at $P_{cw} = 140$ W cm^{-2}. The relationship between [C] and the IQE values for NBE emission indicates that the major NRCs in n-type GaN are carbon in most ranges of [C] from 1×10^{14} to 2×10^{16} cm^{-3}, and the major NRCs switch from carbon impurities to intrinsic NRCs, such as divacancy, when [C] is less than 3.5×10^{14} cm^{-3}.

I am grateful to Dr. Y. Murata for his support in creating the figure.

AUTHOR DECLARATIONS

Conflict of Interest

The authors have no conflicts to disclose.

Author Contributions

K. Sano: Conceptualization (equal); Data curation (equal); Investigation (equal); Methodology (equal); Visualization (equal); Writing – original draft (equal). **H. Fujikura:** Resources (lead); Writing – review & editing (equal). **T. Konno:** Resources (supporting); Writing – review & editing (equal). **S. Kaneki:** Resources (supporting); Writing – review & editing (equal). **S. Ichikawa:** Supervision (supporting); Writing – review & editing (equal). **K. Kojima:** Conceptualization (equal); Methodology (equal); Project administration (equal); Supervision (equal); Writing – review & editing (equal).

DATA AVAILABILITY

The data that support the findings of this study are available from the corresponding author upon reasonable request.

REFERENCES

[1]Y. Narukawa, M. Ichikawa, D. Sanga, M. Sano, and T. Mukai, "White light emitting diodes with super-high luminous efficacy," J. Phys. D **43**, 354002 (2010).
[2]Y. Saitoh, K. Sumiyoshi, M. Okada, T. Horii, T. Miyazaki, H. Shiomi, M. Ueno, K. Katayama, M. Kiyama, and T. Nakamura, "Extremely low on-resistance and high breakdown voltage observed in vertical GaN schottky barrier diodes with high-mobility drift layers on low-dislocation-density GaN substrates," Appl. Phys. Express **3**, 081001 (2010).
[3]J. Kolník, c. H. Oğuzman, K. F. Brennan, R. Wang, P. P. Ruden, and Y. Wang, "Electronic transport studies of bulk zincblende and wurtzite phases of GaN based on an ensemble Monte Carlo calculation including a full zone band structure," J. Appl. Phys. **78**, 1033–1038 (1995).
[4]T. Sugahara, H. Sato, M. Hao, Y. Naoi, S. Kurai, S. Tottori, K. Yamashita, K. Nishino, L. T. Romano, and S. Sakai, "Direct evidence that dislocations are non-radiative recombination centers in GaN," Jpn. J. Appl. Phys., Part 2 **37**, L398 (1998).
[5]K. Motoki, T. Okahisa, S. Nakahata, N. Matsumoto, H. Kimura, H. Kasai, K. Takemoto, K. Uematsu, M. Ueno, Y. Kumagai, A. Koukitu, and H. Seki, "Growth and characterization of freestanding GaN substrates," J. Cryst. Growth **237**, 912–921 (2002).
[6]Y. Oshima, T. Eri, M. Shibata, H. Sunakawa, K. Kobayashi, T. Ichihashi, and A. Usui, "Preparation of freestanding GaN wafers by hydride vapor phase epitaxy with void-assisted separation," Jpn. J. Appl. Phys., Part 2 **42**, L1 (2003).
[7]M. Saito, D. S. Kamber, T. J. Baker, K. Fujito, S. P. DenBaars, J. S. Speck, and S. Nakamura, "Plane dependent growth of GaN in supercritical basic ammonia," Appl. Phys. Express **1**, 121103 (2008).
[8]K. Fujito, S. Kubo, H. Nagaoka, T. Mochizuki, H. Namita, and S. Nagao, "Bulk GaN crystals grown by HVPE," J. Cryst. Growth **311**, 3011–3014 (2009).
[9]R. Dwiliński, R. Doradziński, J. Garczyński, L. Sierzputowski, R. Kucharski, M. Zając, M. Rudziński, R. Kudrawiec, W. Strupiński, and J. Misiewicz, "Ammonothermal GaN substrates: Growth accomplishments and applications," Phys. Status Solidi A **208**, 1489–1493 (2011).
[10]T. Yoshida, Y. Oshima, K. Watanabe, T. Tsuchiya, and T. Mishima, "Ultrahigh-speed growth of GaN by hydride vapor phase epitaxy," Phys. Status Solidi C **8**, 2110–2112 (2011).
[11]Q. Bao, M. Saito, K. Hazu, K. Furusawa, Y. Kagamitani, R. Kayano, D. Tomida, K. Qiao, T. Ishiguro, Y. Chiaki, and S. Chichibu, "Ammonothermal crystal growth of GaN using an NH_4F mineralizer," Cryst. Growth Des. **13**, 4158 (2013).
[12]Y. Mori, M. Imade, M. Maruyama, and M. Yoshimura, "Growth of GaN crystals by Na flux method," ECS J. Solid State Sci. Technol. **2**, N3068 (2013).
[13]Y. Mikawa, T. Ishinabe, S. Kawabata, T. Mochizuki, A. Kojima, Y. Kagamitani, and H. Fujisawa, *Ammonothermal Growth of Polar and Non-Polar Bulk GaN Crystal* (SPIE, 2015), p. 936302.
[14]Y. Tsukada, Y. Enatsu, S. Kubo, H. Ikeda, K. Kurihara, H. Matsumoto, S. Nagao, Y. Mikawa, and K. Fujito, "High-quality, 2-inch-diameter *m*-plane GaN substrates grown by hydride vapor phase epitaxy on acidic ammonothermal seeds," Jpn. J. Appl. Phys., Part 1 **55**, 05FC01 (2016).
[15]S. Pimputkar, J. Speck, and S. Nakamura, "Basic ammonothermal GaN growth in molybdenum capsules," J. Cryst. Growth **456**, 15–20 (2016).
[16]G. Piao, K. Ikenaga, Y. Yano, H. Tokunaga, A. Mishima, Y. Ban, T. Tabuchi, and K. Matsumoto, "Study of carbon concentration in GaN grown by metalorganic chemical vapor deposition," J. Cryst. Growth **456**, 137–139 (2016).
[17]Z. Z. Bandić, P. M. Bridger, E. C. Piquette, and T. C. McGill, "Minority carrier diffusion length and lifetime in GaN," Appl. Phys. Lett. **72**, 3166–3168 (1998).
[18]K. C. Collins, A. M. Armstrong, A. A. Allerman, G. Vizkelethy, S. B. Van Deusen, F. Léonard, and A. A. Talin, "Proton irradiation effects on minority carrier diffusion length and defect introduction in homoepitaxial and heteroepitaxial n-GaN," J. Appl. Phys. **122**, 235705 (2017).
[19]J. Wang, X. Wang, J. Chen, X. Gao, X. Zeng, H. Mao, and K. Xu, "Investigation on minority carrier lifetime, diffusion length and recombination mechanism of Mg-doped GaN grown by MOCVD," J. Alloys Compd. **870**, 159477 (2021).
[20]F. Horikiri, Y. Narita, T. Yoshida, T. Kitamura, H. Ohta, T. Nakamura, and T. Mishima, "Wafer-level nondestructive inspection of substrate off-angle and net donor concentration of the n^--drift layer in vertical GaN-on-GaN schottky diodes," Jpn. J. Appl. Phys., Part 1 **56**, 061001 (2017).
[21]L. Jiang, J. Liu, A. Tian, X. Ren, S. Huang, W. Zhou, L. Zhang, D. Li, S. Zhang, M. Ikeda *et al.*, "Influence of substrate misorientation on carbon impurity incorporation and electrical properties of p-GaN grown by metalorganic chemical vapor deposition," Appl. Phys. Express **12**, 055503 (2019).
[22]J. L. Lyons, A. Janotti, and C. G. Van de Walle, "Effects of carbon on the electrical and optical properties of InN, GaN, and AlN," Phys. Rev. B **89**, 035204 (2014).
[23]M. Matsubara and E. Bellotti, "A first-principles study of carbon-related energy levels in GaN. I. Complexes formed by substitutional/interstitial carbons and gallium/nitrogen vacancies," J. Appl. Phys. **121**, 195701 (2017).
[24]S. G. Christenson, W. Xie, Y. Y. Sun, and S. B. Zhang, "Carbon as a source for yellow luminescence in GaN: Isolated CN defect or its complexes," J. Appl. Phys. **118**, 135708 (2015).
[25]J. L. Lyons, A. Janotti, and C. G. Van de Walle, "Carbon impurities and the yellow luminescence in GaN," Appl. Phys. Lett. **97**, 152108 (2010).
[26]T. Ogino and M. Aoki, "Mechanism of yellow luminescence in GaN," Jpn. J. Appl. Phys., Part 1 **19**, 2395 (1980).
[27]H. Tang, J. B. Webb, J. A. Bardwell, S. Raymond, J. Salzman, and C. Uzan-Saguy, "Properties of carbon-doped GaN," Appl. Phys. Lett. **78**, 757–759 (2001).
[28]C. H. Seager, A. F. Wright, J. Yu, and W. Götz, "Role of carbon in GaN," J. Appl. Phys. **92**, 6553–6560 (2002).
[29]R. Armitage, W. Hong, Q. Yang, H. Feick, J. Gebauer, E. R. Weber, S. Hautakangas, and K. Saarinen, "Contributions from gallium vacancies and carbon-related defects to the 'yellow luminescence' in GaN," Appl. Phys. Lett. **82**, 3457–3459 (2003).
[30]R. Armitage, Q. Yang, and E. R. Weber, "Analysis of the carbon-related 'blue' luminescence in GaN," J. Appl. Phys. **97**, 073524 (2005).
[31]M. A. Reshchikov and H. Morkoç, "Luminescence properties of defects in GaN," J. Appl. Phys. **97**, 061301 (2005).
[32]M. A. Reshchikov, D. O. Demchenko, J. D. McNamara, S. Fernández-Garrido, and R. Calarco, "Green luminescence in Mg-doped GaN," Phys. Rev. B **90**, 035207 (2014).
[33]M. A. Reshchikov, M. Vorobiov, D. O. Demchenko, U. Özgür, H. Morkoç, A. Lesnik, M. P. Hoffmann, F. Hörich, A. Dadgar, and A. Strittmatter, "Two charge states of the C_N acceptor in GaN: Evidence from photoluminescence," Phys. Rev. B **98**, 125207 (2018).
[34]M. A. Reshchikov, J. D. McNamara, H. Helava, A. Usikov, and Y. Makarov, "Two yellow luminescence bands in undoped GaN," Sci. Rep. **8**, 8091 (2018).
[35]K. Kojima, F. Horikiri, Y. Narita, T. Yoshida, H. Fujikura, and S. F. Chichibu, "Roles of carbon impurities and intrinsic nonradiative recombination centers on the carrier recombination processes of GaN crystals," Appl. Phys. Express **13**, 012004 (2019).
[36]D. V. Lang, "Deep-level transient spectroscopy: A new method to characterize traps in semiconductors," J. Appl. Phys. **45**, 3023–3032 (1974).
[37]D. Haase, M. Schmid, W. Kürner, A. Dörnen, V. Härle, F. Scholz, M. Burkard, and H. Schweizer, "Deep-level defects and n-type-carrier concentration in nitrogen implanted GaN," Appl. Phys. Lett. **69**, 2525–2527 (1996).
[38]A. Armstrong, A. R. Arehart, D. Green, U. K. Mishra, J. S. Speck, and S. A. Ringel, "Impact of deep levels on the electrical conductivity and luminescence of gallium nitride codoped with carbon and silicon," J. Appl. Phys. **98**, 053704 (2005).
[39]U. Honda, Y. Yamada, Y. Tokuda, and K. Shiojima, "Deep levels in n-GaN doped with carbon studied by deep level and minority carrier transient spectroscopies," Jpn. J. Appl. Phys., Part 1 **51**, 04DF04 (2012).
[40]T. Tanaka, K. Shiojima, T. Mishima, and Y. Tokuda, "Deep-level transient spectroscopy of low-free-carrier-concentration n-GaN layers grown on free-standing GaN substrates: Dependence on carbon compensation ratio," Jpn. J. Appl. Phys., Part 1 **55**, 061101 (2016).
[41]H. Yamada, H. Chonan, T. Takahashi, T. Yamada, and M. Shimizu, "Deep-level traps in lightly Si-doped n-GaN on free-standing m-oriented GaN substrates," AIP Adv. **8**, 045311 (2018).

[42]K. Kanegae, H. Fujikura, Y. Otoki, T. Konno, T. Yoshida, M. Horita, T. Kimoto, and J. Suda, "Deep-level transient spectroscopy studies of electron and hole traps in n-type GaN homoepitaxial layers grown by quartz-free hydride-vapor-phase epitaxy," Appl. Phys. Lett. **115**, 012103 (2019).
[43]G. Alfieri and V. K. Sundaramoorthy, "Defect energy levels in carbon implanted n-type homoepitaxial GaN," J. Appl. Phys. **126**, 125301 (2019).
[44]T. Narita, M. Horita, K. Tomita, T. Kachi, and J. Suda, "Why do electron traps at E_C −0.6 eV have inverse correlation with carbon concentrations in n-type GaN layers?," Jpn. J. Appl. Phys., Part 1 **59**, 105505 (2020).
[45]Y. Zhang, Z. Chen, W. Li, H. Lee, M. R. Karim, A. R. Arehart, S. A. Ringel, S. Rajan, and H. Zhao, "Probing unintentional Fe impurity incorporation in MOCVD homoepitaxy GaN: Toward GaN vertical power devices," J. Appl. Phys. **127**, 215707 (2020).
[46]F. Kaess, S. Mita, J. Xie, P. Reddy, A. Klump, L. H. Hernandez-Balderrama, S. Washiyama, A. Franke, R. Kirste, A. Hoffmann, R. Collazo, and Z. Sitar, "Correlation between mobility collapse and carbon impurities in Si-doped GaN grown by low pressure metalorganic chemical vapor deposition," J. Appl. Phys. **120**, 105701 (2016).
[47]T. Kimura, T. Konno, and H. Fujikura, "Substantial and simultaneous reduction of major electron traps and residual carbon in homoepitaxial GaN layers," Appl. Phys. Lett. **118**, 182104 (2021).
[48]A. Ishitani, K. Okuno, A. Karen, S. Karen, and F. Soeda, in Proceedings of International Conference on Materials and Process Characterization for VLSI, 1988.
[49]M. Sumiya, K. Yoshimura, K. Ohtsuka, and S. Fuke, "Dependence of impurity incorporation on the polar direction of GaN film growth," Appl. Phys. Lett. **76**, 2098–2100 (2000).
[50]N. Fichtenbaum, T. Mates, S. Keller, S. DenBaars, and U. Mishra, "Impurity incorporation in heteroepitaxial n-face and Ga-face GaN films grown by metal-organic chemical vapor deposition," J. Cryst. Growth **310**, 1124–1131 (2008).
[51]K. Kojima, T. Ohtomo, K. Ikemura, Y. Yamazaki, M. Saito, H. Ikeda, K. Fujito, and S. F. Chichibu, "Determination of absolute value of quantum efficiency of radiation in high quality GaN single crystals using an integrating sphere," J. Appl. Phys. **120**, 015704 (2016).
[52]D. Wickramaratne, J.-X. Shen, C. E. Dreyer, M. Engel, M. Marsman, G. Kresse, S. Marcinkevičius, A. Alkauskas, and C. G. Van de Walle, "Iron as a source of efficient Shockley-Read-Hall recombination in GaN," Appl. Phys. Lett. **109**, 162107 (2016).
[53]K. Kojima, H. Ikeda, K. Fujito, and S. F. Chichibu, "Demonstration of omnidirectional photoluminescence (ODPL) spectroscopy for precise determination of internal quantum efficiency of radiation in GaN single crystals," Appl. Phys. Lett. **111**, 032111 (2017).
[54]M. A. Reshchikov, D. O. Demchenko, A. Usikov, H. Helava, and Y. Makarov, "Carbon defects as sources of the green and yellow luminescence bands in undoped GaN," Phys. Rev. B **90**, 235203 (2014).
[55]W. P. Dumke, "Spontaneous radiative recombination in semiconductors," Phys. Rev. **105**, 139–144 (1957).
[56]P. Asbeck, "Self-absorption effects on the radiative lifetime in GaAs-GaAlAs double heterostructures," J. Appl. Phys. **48**, 820–822 (1977).
[57]J. Neugebauer and C. G. Van de Walle, "Gallium vacancies and the yellow luminescence in GaN," Appl. Phys. Lett. **69**, 503–505 (1996).
[58]K. Saarinen, T. Laine, S. Kuisma, J. Nissilä, P. Hautojärvi, L. Dobrzynski, J. M. Baranowski, K. Pakula, R. Stepniewski, M. Wojdak, A. Wysmolek, T. Suski, M. Leszczynski, I. Grzegory, and S. Porowski, "Observation of native Ga vacancies in GaN by positron annihilation," Phys. Rev. Lett. **79**, 3030–3033 (1997).
[59]K. Kojima and S. F. Chichibu, "Urbach-martienssen tail as the origin of the two-peak structure in the photoluminescence spectra for the near-band-edge emission of a freestanding GaN crystal observed by omnidirectional photoluminescence spectroscopy," Appl. Phys. Lett. **117**, 171103 (2020).
[60]K. Kojima, K. Ikemura, K. Matsumori, Y. Yamada, Y. Kanemitsu, and S. F. Chichibu, "Internal quantum efficiency of radiation in a bulk $CH_3NH_3PbBr_3$ perovskite crystal quantified by using the omnidirectional photoluminescence spectroscopy," APL Mater. **7**, 071116 (2019).
[61]K. Kojima and S. F. Chichibu, "Correlation between the internal quantum efficiency and photoluminescence lifetime of the near-band-edge emission in a ZnO single crystal grown by the hydrothermal method," Appl. Phys. Express **13**, 121005 (2020).
[62]S. F. Chichibu, A. Uedono, K. Kojima, H. Ikeda, K. Fujito, S. Takashima, M. Edo, K. Ueno, and S. Ishibashi, "The origins and properties of intrinsic nonradiative recombination centers in wide bandgap GaN and AlGaN," J. Appl. Phys. **123**, 161413 (2018).
[63]S. F. Chichibu, K. Hazu, Y. Ishikawa, M. Tashiro, H. Namita, S. Nagao, K. Fujito, and A. Uedono, "Time-resolved photoluminescence, positron annihilation, and $Al_{0.23}Ga_{0.77}N$/GaN heterostructure growth studies on low defect density polar and nonpolar freestanding GaN substrates grown by hydride vapor phase epitaxy," J. Appl. Phys. **111**, 103518 (2012).
[64]K. Kawakami, T. Nakano, and A. A. Yamaguchi, Proc. SPIE **9748**, 97480S (2016).
[65]S. Ichikawa, Y. Matsuda, H. Dojo, M. Funato, Y. Kawakami, and K. Kojima, in The 14th International Conference on Nitride Semiconductors, 2023.